Magnetic momentum density, Fermi surface, and directional magnetic Compton profiles in $LaSr_2Mn_2O_7$ and $La_{1.2}Sr_{1.8}Mn_2O_7$

P. E. Mijnarends,[1,2] S. Kaprzyk,[1,3] B. Barbiellini,[1] Yinwan Li,[4,5] J. F. Mitchell,[5] P. A. Montano,[4,6] and A. Bansil[1]
[1]*Physics Department, Northeastern University, Boston, Massachusetts 02115, USA*
[2]*Department of Radiation, Radionuclides & Reactors, Faculty of Applied Sciences, Delft University of Technology, Delft, The Netherlands*
[3]*Academy of Mining and Metallurgy AGH, 30059 Krakow, Poland*
[4]*Department of Physics, University of Illinois, Chicago, Illinois 60680, USA*
[5]*Materials Science Division, Argonne National Laboratory, Argonne, Illinois 60439, USA*
[6]*Scientific User Facilities Division, U.S. Department of Energy, 1000 Independence Avenue, Washington DC 20585-1290, USA*
(Received 3 November 2006; published 23 January 2007)

We have carried out first principles, all-electron computations of the magnetic momentum density $\rho_{mag}(\mathbf{p})$ and magnetic Compton profiles (MCPs) for momentum transfer along the [100], [001], and [110] directions in $LaSr_2Mn_2O_7$ and $La_{1.2}Sr_{1.8}Mn_2O_7$ within the local spin density approximation (LSDA) based band theory framework. Parallel measurements of these three MCPs from a single crystal of $La_{1.2}Sr_{1.8}Mn_2O_7$ at 5 K in a magnetic field of 7 T are also reported. $\rho_{mag}(\mathbf{p})$ is shown to contain distinct peaks arising from the occupied majority-spin t_{2g} electrons and to display images of the Fermi surface (FS) in the first and higher Brillouin zones (BZs). The overall shape of the MCPs, $J_{mag}(p_z)$, obtained by integrating $\rho_{mag}(\mathbf{p})$ over p_x and p_y, is found to be dominated by the majority-spin t_{2g} states. The FS-related fine structure in the MCPs is, however, substantial only in the [100] MCP, which contains features arising from the large majority-spin hole sheets. The overall shapes and widths of the experimental MCPs along all three directions investigated are in reasonably good accord with theoretical predictions, although some discrepancies indicating inadequacy of the LSDA in treating the magnetic states can be identified. We discuss details of the FS-related signatures in the first and higher BZs in the [100] MCP and show that high resolution magnetic Compton scattering experiments with a momentum resolution of 0.1 a.u. full-width-at-half-maximum or better will be necessary to observe this fine structure. We comment also on the feasibility of using positron annihilation spectroscopy in this connection.

DOI: 10.1103/PhysRevB.75.014428 PACS number(s): 75.47.Lx, 78.70.Ck, 71.18.+y, 75.47.Gk

I. INTRODUCTION

Layered manganites have drawn a great deal of attention as model systems which display a wide range of electric and magnetic properties and undergo a variety of phase transitions related to the interplay between the charge, spin, and orbital degrees of freedom as a function of temperature and doping. The recent revival of interest in the manganites is partly due to their structural resemblence to the cuprates. The structure is given by the general formula $(La_{1-x}Sr_xMnO_3)_nSrO$ (LSMO) and consists of n layers of corner sharing MnO_6 octahedra, separated by insulating (La,Sr)O layers. The manganites show various degrees of colossal magnetoresistance (CMR) effect. For example, in the $n=2$ bilayer material $La_{1.2}Sr_{1.8}Mn_2O_7$ (i.e., $x=0.40$) investigated in this study, the CMR effect is a factor of ~ 200 at 129 K (just above the Curie temperature $T_c \sim 120$ K) under a magnetic field of 7 T, and even at low fields the resistance changes by $\sim 200\%$.[1] Neutron studies[2] in this compound show that below T_c the spins are aligned ferromagnetically within a MnO plane and antiferromagnetically canted between two planes within a double layer.

Compton scattering refers to inelastic x-ray scattering in the deeply inelastic regime and it is well known that this technique provides a unique probe of the correlated many-body ground state wave function of the electronic system via a measurement of the associated momentum density. In comparison to other **k**-resolved spectroscopies, Compton scattering possesses the advantages that it is neither surface sensitive as photoemission is, nor defect sensitive as de Haas–van Alphen or positron annihilation. The possibility of using magnetic Compton scattering (MCS) to determine the momentum distribution of magnetic electrons was recognized quite early,[3,4] but the scattering cross section in the magnetic channel is typically several orders of magnitude smaller than for charge scattering. For this reason, MCS experiments have become practical only in the last few years with the availability of high-energy, circularly polarized, x rays at the synchrotron light sources.

This article presents all-electron, first-principles computations of the magnetic Compton profiles (MCPs) in $LaSr_2Mn_2O_7$ and $La_{1.2}Sr_{1.8}Mn_2O_7$ within the LSDA-based band theory framework. Theoretical predictions for a scattering vector along the three high-symmetry directions [100], [001], and [110], are compared and contrasted with corresponding measurements of the MCPs taken from a $La_{1.2}Sr_{1.8}Mn_2O_7$ single crystal at 5 K under a magnetic field of 7 T. Our study provides a benchmark for assessing electron correlation effects beyond the conventional LSDA framework on the magnetic momentum density, following up on earlier work on many nonmagnetic materials.[5] We delineate the nature of the Fermi surface (FS) generated structure in the magnetic momentum density and discuss how this structure is reflected in the MCPs for various directions of the x-ray scattering vector. All existing MCP data on La manganite—including the MCP data presented in this

article—have been taken at a momentum resolution of around 0.4 a.u. full width at half maximum (FWHM). We will show, however, that this level of resolution is not sufficient for investigating FS signatures in the MCPs and that for this purpose higher resolution experiments are needed. In this connection, applicability of the positron annihilation spectroscopy is also considered. These results will serve to guide future efforts aimed at exploring FS signatures in La manganite via high-resolution MCP and positron annihilation experiments.

Concerning relevant previous magnetic Compton scattering studies on La manganite, Li *et al.*[6] have focused on the [110] MCP in $La_{1.2}Sr_{1.8}Mn_2O_7$ and shown that the shape of the [110] MCP contains a remarkable signature of the occupancy of the $d_{x^2-y^2}$ electrons. By using a high magnetic field of 7 T to maintain an electronically homogeneous phase, these authors demonstrate that changes with temperature in the number of $d_{x^2-y^2}$ orbitals can be deduced from the [110] MCPs measured at different temperatures. Koizumi *et al.*[7,8] have investigated the doping dependence of the [100] and [001] MCPs in La manganite under a relatively low magnetic field of 2.5 T. They analyze their MCPs in terms of atomic and cluster type computations of the momentum density to gain insight into the occupation of magnetic orbitals in the system but do not obtain detailed FS information.

By way of brief background, we note that the magnetic momentum density $\rho_{\mathrm{mag}}(\mathbf{p})$ is given by

$$\rho_{\mathrm{mag}}(\mathbf{p}) = \rho_{\uparrow}(\mathbf{p}) - \rho_{\downarrow}(\mathbf{p}), \tag{1}$$

where[9]

$$\rho_{\uparrow(\downarrow)}(\mathbf{p}) = \sum_i n_i^{\uparrow(\downarrow)} \left| \int \psi_i^{\uparrow(\downarrow)}(\mathbf{r}) \exp(-i\mathbf{p}\cdot\mathbf{r}) d\mathbf{r} \right|^2 \tag{2}$$

is the spin-polarized momentum density of a system of electrons in states i with wave functions ψ_i and occupation numbers n_i. The Fourier transforms of the wave functions generally vary smoothly with momentum. The occupation function, on the other hand, introduces discontinuities in $\rho_{\uparrow}$ and $\rho_{\downarrow}$ at the Fermi momenta and at the Umklapp images of the FS at higher momenta with appropriate weights.

The quantity of interest in a magnetic Compton scattering experiment is the double differential magnetic scattering cross section, given by[10,11]

$$\frac{d^2\sigma_m}{d\Omega d\omega_2} = \frac{r_e^2}{2}\left(\frac{\omega_2}{\omega_1}\right)^2 P_c \frac{\omega_1}{m_e c^2}(\cos\theta - 1)\left[\cos\alpha\cos\theta + \left(\frac{\omega_2}{\omega_1}\right)\cos(\alpha-\theta)\right] J_{\mathrm{mag}}(p_z), \tag{3}$$

where P_c is the degree of circular polarization, θ is the scattering angle, and $\omega_1(\omega_2)$ is the photon energy before (after) scattering. α is the angle between the spin (assumed to lie in the scattering plane) and the momentum of the incident photon, m_e is the electron rest mass, and r_e is the classical electron radius. Finally, the MCP $J_{\mathrm{mag}}(p_z)$ is defined as the difference between the Compton profiles for the majority (↑) and minority (↓) spin profiles $J_{\uparrow}$ and $J_{\downarrow}$:

$$J_{\mathrm{mag}}(p_z) = J_{\uparrow}(p_z) - J_{\downarrow}(p_z) = \int\int [\rho_{\uparrow}(\mathbf{p}) - \rho_{\downarrow}(\mathbf{p})] dp_x dp_y. \tag{4}$$

It should be noted that $J_{\mathrm{mag}}(p_z)$ only involves unpaired electron spins. Unlike neutron scattering, the magnetic Compton experiment does not couple to the orbital moment.

The remainder of this article is organized as follows. Section II describes experimental details. In Sec. III we discuss earlier band-structure studies on the 327 and 113 manganites, followed by particulars of our electronic structure calculations based on the Korringa-Kohn-Rostoker (KKR) method to obtain spin-polarized energy bands, Fermi surfaces, momentum densities, and the MCPs. Section IV A briefly presents band-structure results, while Sec. IV B considers the Fermi surface, the way it changes under doping, and the possible role it plays in the occurrence of structural and magnetic instabilities. The spin-dependent momentum density and the MCPs are presented in Sec. IV C. Section IV D discusses in how far positron annihilation may be able to shed further light on details of the Fermi surface. The article concludes with a summary of the results in Sec. V.

II. EXPERIMENTS

Circularly polarized photons were produced using an elliptical multipole wiggler (EMW) at beamline 11-ID-B (BESSRC) of the Advanced Photon Source at Argonne National Laboratory. The horizontal field in the EMW is produced by electromagnets so that the degree of polarization P_c can be tuned by adjusting the current through the magnets.[12] This allows optimization of the figure of merit $P_c\sqrt{I}$ (where I is the intensity of the beam) and easy reversal of the polarization, important when working at high magnetic fields where fast switching of the field is difficult. The Laue monochromator consisted of an annealed Si(220) crystal, 10 mm wide and 10 mm thick, mounted on a water-cooled Ni-plated Cu support in Ga. In addition, a water-cooled Cu filter was mounted in front of the crystal to reduce the heat load. The sample was mounted inside the cryostat and could be magnetized by a field of up to 8 T generated by an Oxford Instruments Spectromag superconducting magnet. The temperature at the sample position could be varied from 1.7 to 300 K. The sample was a high-quality single crystal of $La_{1.2}Sr_{1.8}Mn_2O_7$ measuring $10\times5\times2$ mm^3 with its shortest side along the crystalline c axis. It was fixed to the holder by a high-purity aluminum clip to avoid magnetic contamination. The x-ray beam intersects neither the holder nor the clip. A motorized slit was placed in the beam close to the sample. Its size was chosen to fit the sample dimensions in order to maximize the figure of merit. The scattering angle θ was set at 170°, while the magnetic field was oriented at an angle of α=176° with respect to the incident beam. The scattered photons were detected by a three-element Ge solid-state detector with a resolution of 0.4 keV at 100 keV. All measurements reported here were performed at 125 keV. Magnetic Compton profiles were obtained using magnetic fields of 3 and 7 T along the three high-symmetry directions [001], [100], and [110] at temperatures of 5, 100, 160, and

200 K, which straddle the Curie temperature $T_c = 120$ K. In this article only the 5 K, 7 T measurements will be discussed as these are magnetically homogeneous and therefore the most relevant. The momentum resolution was 0.4 a.u. FWHM.

III. COMPUTATIONS

A. Earlier band-structure studies

There exist only a few studies of the electronic structure of the bilayer manganites. De Boer and de Groot[13,14] performed a full-potential LAPW calculation of the electronic structure of $LaSr_2Mn_2O_7$ using the structural data of Seshadri *et al.*[15] Exchange-correlation effects were incorporated within the framework of the generalized gradient approximation (GGA).[16] These authors obtained a metallic majority-spin band while the minority-spin band is reminiscent of a doped semiconductor with a band gap of 1.7 eV. The Fermi level lies slightly above the bottom of the minority-spin conduction band, yielding a nearly half-metallic ferromagnet. The total spin magnetic moment per formula unit is found to be $6.995\mu_B$. (If the Fermi level were lying in the gap the magnetic moment would be $7\mu_B$.) Huang *et al.*[17] calculated the electronic structure of $La_{2-2x}Sr_{1+2x}Mn_2O_7$ for x between[18] 0.3 and 0.5 for different lattice parameters,[19] using the full-potential linear muffin-tin orbital (LMTO) method[20,21] with the Ceperly-Alder exchange-correlation functional.[22] They used the virtual crystal approximation (VCA) to treat the effect of La/Sr substitution and also found the material to be (nearly) half-metallic for x between 0.4 and 0.5. These authors also computed the Fermi surface which was found to be strongly two dimensional. The question of whether $La_{1.2}Sr_{1.8}Mn_2O_7$ is a half-metallic ferromagnet or not is still a controversial one. As noted above, the band structure of Ref. 13 shows small minority-spin pockets at Γ, whereas they seem to be absent in Ref. 17. Recent angle-resolved photoemission studies[23] may directly support their existence.

More work has been done on the related perovskite manganites of general formula $La_{1-x}(Ca,Sr)_xMnO_3$, which also show the CMR effect. Pickett and Singh[24,25] have shown that an LSDA calculation for the undoped end-compound $LaMnO_3$ using a five atom perovskite unit cell produces a ferromagnetic (FM) ground state. However, if a 20 atom $\sqrt{2}\times 2\times\sqrt{2}$ *Pnma* supercell is used and the structure is allowed to relax [resulting in rotations of the O octahedra and Jahn-Teller (JT) distortions], a small band gap opens, in combination with new band splittings and shifts. As a result, the ground state is found to be an *A*-type antiferromagnetic (AFM) insulator (spin aligned in layers, alternating from layer to layer[26]) in agreement with experiment. $CaMnO_3$, on the other hand, is correctly found to be a *G*-type AFM insulator with a narrow band gap and a rocksalt arrangement of moments. Thus, the LSDA produces the right ground state in both cases.

As $LaMnO_3$ is hole-doped by partial substitution of La^{3+} by a divalent element (Ca, Sr, Ba) ($x \approx 0.33$, the region where CMR occurs), the ground state becomes ferromagnetic with rotated octahedra but no JT distortion.[25] Since the Mn *d* band is now less than half occupied the Fermi level E_F is not close to a (pseudo) band gap for the majority-spin electrons and the material is a metal. Livesay *et al.*[27] have calculated the electronic structure of $La_{0.7}Sr_{0.3}MnO_3$ and performed positron annihilation measurements of the Fermi surface. They find a FS consisting of hole cuboids centered at *R* (coined "woolsacks" by the authors) and an electron spheroid centered at Γ, which touches the woolsacks along the [111] directions. This FS can be viewed as a three-dimensional analogue of the two-dimensional FS found in $La_{2-2x}Sr_{1+2x}Mn_2O_7$ (see also Sec. IV B). Similar to its 2D equivalent, the presence of flat parts of the FS opens the possibility of nesting. Other similarities may be found in the density of states. All these calculations agree on the presence of small minority-spin electron pockets, similar to those resulting from electronic structure calculations on 327-LSMO. Also, point-contact Andreev reflection measurements[28] on $La_{0.7}Sr_{0.3}MnO_3$ have shown the presence of minority-spin electrons at the FS. Finally, we performed LSDA calculations of the FM phases of both $LaMnO_3$ and $LaSr_2Mn_2O_7$. The projected densities of states for these FM cases look very similar. For the majority-spin channel the Mn 3*d* states of both compounds form bands between −2.5 eV and +2.5 eV with respect to E_F. The e_g bands are rather broad compared to the t_{2g} bands, cross E_F, and are therefore only partly filled. The exchange interaction places them 2.5 eV higher in energy than the majority-spin states. In summary, important differences between the two classes of materials notwithstanding, there are also strong parallels to be found.

B. Present work

In order to obtain the Fermi surface, momentum densities and Compton profiles, the electronic structure of $LaSr_2Mn_2O_7$ was first obtained within an all-electron fully charge and spin self-consistent KKR framework.[29–33] The formalism for computing momentum densities is discussed in Refs. 34–38. The structure data were taken from Seshadri *et al.*[15] for the space group $I4/mmm$ (No. 139).[39] Two empty spheres per formula unit were inserted to increase the filling factor. The maximum angular momentum cutoff $l_{\max}$ was 3 for all atoms.[40] Exchange-correlation effects were incorporated within the von Barth-Hedin local spin density approximation (LSDA).[41] The self-consistency cycles were repeated until the maximum difference between the input and output potentials was less than 10^{-5} Ry. Parallel to this, we have also carried out full-potential computations within both the KKR and the LAPW schemes in order to ascertain that the band structure and Fermi surface underlying our momentum density and MCP computations is essentially the same as the full-potential results. Moreover, we have carried out self-consistent computations on $La_{1.2}Sr_{1.8}Mn_2O_7$ within the VCA scheme to study the effect of La/Sr substitution, and find that the rigid band approximation is appropriate. However, there might be some uncertainty with regard to where the doped magnetic electrons should go. We have modeled the effect by simply adding the extra 0.2 electrons per formula unit exclusively into the majority spin band, which is similar to the viewpoint argued by Huang *et al.*[17] and in keeping with the

spirit of Hund's rules. In principle, one could imagine that some of the added electrons will in fact get added into the minority spin bands and in that case the effect of doping on the majority sheets will be reduced.

The spin dependent momentum density was computed on a regular mesh in **p** space, created by translating 765 uniformly spaced **k** points in the 1/16-th irreducible wedge of the Brillouin zone via 36 000 reciprocal lattice vectors **G** each (i.e., Umklapp processes $\mathbf{p}=\mathbf{k}+\mathbf{G}$). Thus, the resulting mesh size is $\Delta p_x=\Delta p_y=0.02681$ a.u. and $\Delta p_z=0.04157$ a.u., with the mesh filling a sphere of radius 14.9 a.u. This dataset of band-by-band $\rho_\uparrow(\mathbf{p})$ and $\rho_\downarrow(\mathbf{p})$ values over the aforementioned mesh in **p** space forms the basis for obtaining the directional MCPs and 2D projections for the stoichiometric compound. By moving the Fermi level for the majority-spin electrons up by 20 mRy to account for the extra electrons, the same dataset is used to repeat the computations for the doped compound.

IV. RESULTS AND DISCUSSION

A. Band structure

There is a good overall agreement between our band structure and the results of Refs. 13 and 17. All three computations agree on a nearly halfmetallic ferromagnetic band structure with the Fermi level crossing Mn *d* bands. In all computations the majority-spin bands are metallic with a Fermi surface consisting of three sheets. An analysis of the wave functions indicates that the majority-spin bands at E_F mainly involve a mixture of La and Mn e_g, and Sr and O *s*-*p* states, although the O 2*p* and Mn t_{2g} character increases rapidly as one moves to higher binding energies. On the whole, there is little dispersion in the *c* direction, so that the electronic structure is largely two dimensional. The minority conduction band, which near Γ dips below E_F, consists of two nearly degenerate bands (0.7 mRy apart at Γ) of antibonding Mn d_{xy} character. Overall, the minority-spin band structure is similar to that of a doped n-type semiconductor with E_F intersecting the bottom of the conduction band.[42]

B. Fermi surface

Figure 1 shows cross sections of the Fermi surface at five different k_z values for the stoichiometric compound $LaSr_2Mn_2O_7$ ($x=0.5$) as well as the doped material $La_{1.2}Sr_{1.8}Mn_2O_7$ ($x=0.4$).[43] Although the two sets of FSs are similar in shape, doping by substituting La for Sr increases the electron count and thus changes FS dimensions. Both FSs show three sheets for the majority-spin electrons, which consist of two large hole cylinders centered around the *X* $(\pi/a,\pi/a)$ points (red and blue contours), and one squarish Γ-centered electron pillar (black contours).[40] The arrows indicate how the contours change with increasing k_z. For example, the Γ-centered majority-spin electron pillar (black lines) in (a) decreases in size with increasing k_z. One set of majority spin hole cylinders has a squarish cross section with small k_z dispersion near the corners (blue lines), while the other set (red lines) displays strongly rounded corners and no noticeable k_z dispersion. The two small Γ-centered circles in (a) and (b) depict the two dispersionless minority-spin sheets, which have the form of circular pillars.

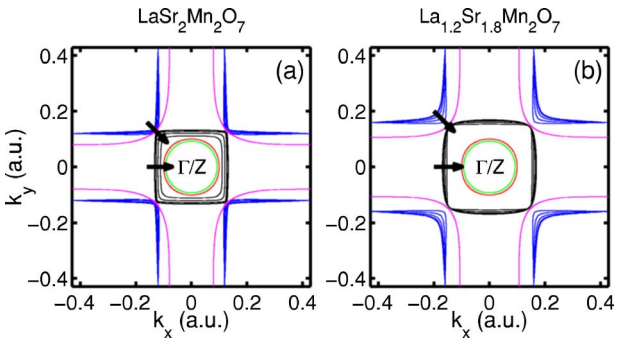

FIG. 1. (Color online) Fermi surface of (a) $LaSr_2Mn_2O_7$ and (b) $La_{1.2}Sr_{1.8}Mn_2O_7$. For each FS sheet five intersections with $(00k_z)$ planes are shown for k_z at Γ, k_z at $Z=(0,0,2\pi/c)$, and k_z at three points between Γ and *Z*. Some intersections are indistinguishable from each other due to the lack of k_z dispersion. Arrows indicate how the FS cross section changes with increasing k_z. Blue and red lines give the two majority spin hole sheets; the squarish feature in the center (black lines) is the majority spin electron pillar. The two circular FS sheets at the center (red and green lines) are the minority-spin electron pillars.

The flatness of some of the FS sheets of undoped LSMO gives rise to Fermi-surface nesting, which can drive structural or magnetic instablities. For instance, the flat parts of the *X*-centered hole cylinders span nesting vectors **q** between $\sim(0.18,0)2\pi/a$ and $(0.28,0)2\pi/a$, and have been implicated in giving rise to an incommensurate charge density wave in the *x* and *y* directions, coupled with Jahn-Teller distortions.[44,45] With doping [Fig. 1(b)], both these hole cylinders become smaller and the splitting between the two hole cylinders increases. There also are changes in the shapes of the various FS sheets with doping (e.g., the blue hole cylinder becomes more rounded at corners in the $k_z=0$ plane and the black electron cylinders become more bulged on the sides), and associated changes in the nesting properties of the FS.

The flat nature of parts of the Fermi surface, together with its pronounced two-dimensional character, also make LSMO an obvious candidate for observation of the FS via the MCS technique. Since according to Eq. (2) the momentum density is not only determined by the occupation function but also by the wave function transforms, we investigate in the following section how the interplay between FS and wave functions affects the observability of various FS sheets. The complete Fermi surface can in principle be mapped without the interference of wave function effects by performing a 2D or 3D reconstruction of the momentum density followed by Lock-Crisp-West folding as described by Matsumoto *et al.*[46] for Al-3 at. % Li alloys. In this way, one can transform the momentum density in **p** space to an occupation number density in **k** space.

C. Magnetic Compton profiles

The MCPs are obtained from the 3D magnetic momentum density $\rho_{\mathrm{mag}}(\mathbf{p})$ via Eq. (4). It is useful, however, to take an

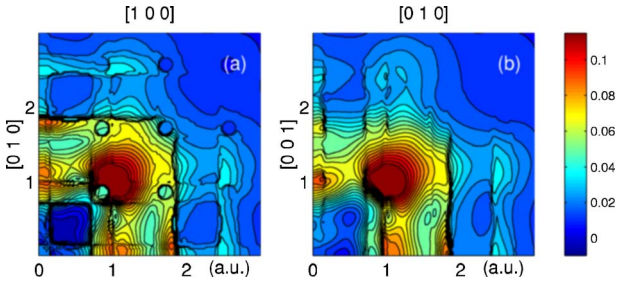

FIG. 2. (Color online) 2D projections of the magnetic momentum density $\rho_{mag}(\mathbf{p})$ for the doped material $La_{1.2}Sr_{1.8}Mn_2O_7$ onto (a) the (001) plane and (b) the (100) plane.

intermediate step and first consider 2D projections along various high-symmetry directions by performing only one of the two integrations involved in Eq. (4). Such a 2D distribution can be obtained by reconstructing $\rho_{mag}(\mathbf{p})$ from a series of measured MCPs and, excepting for effects of the nonuniform positron spatial distribution, it is also measured in a 2D angular correlation of positron annihilation radiation (2D-ACAR) experiment.[47] A $(\gamma, e\gamma)$ experiment where the kinematics of the scattered photon is measured in coincidence with that of the outgoing recoil electron can also access this 2D distribution in principle.[48–50]

Figure 2 shows 2D projections of $\rho_{mag}(\mathbf{p})$ in the doped material onto the (001) and (100) planes. Note that Fermi breaks occur in the momentum density in the first as well as higher BZs, the latter due to Umklapp processes. The size of each break depends on the matrix element of the band intersecting the Fermi surface. Some Fermi breaks are therefore clearly seen while others are hardly visible. In general the breaks are largest in the second and third BZ as a consequence of the predominant d character of the electrons at the Fermi energy in the manganite.[51] We now consider the (001) projection in Fig. 2(a) and focus on signatures therein of various FS sheets of Fig. 1(b). Some of the flat faces of the large majority spin hole-cylinders and their Umklapp images in higher BZs are seen clearly. The splitting between the two types of large hole cylinders (~0.04 a.u.) is difficult to see on the scale of the figure. With regard to the Γ-centered squarish majority-spin electron pillar, two sides of this pillar are visible near the little circular feature located at (0.858, 0.858) a.u. This feature is one of a system of small circular features located on a square mesh of interval 0.858 a.u. They arise from the small minority-spin electron pillars at Γ (see Fig. 1) and are particularly noticeable along the [110] direction and its vicinity, consistent with the d_{xy} symmetry of the underlying wave functions.[52,53] In the following we shall see that the minority-spin pillars are too small to survive the second integration in Eq. (4) and do not produce a measurable signature in the MCPs. The question of their observability through positron annihilation spectroscopy is considered in Sec. IV D below. The results of Fig. 2(b), which gives the (100) projection of the magnetic momentum density, can be interpreted along lines very similar to the preceding discussion of the (001) projection. The presence of clear vertical features in Fig. 2(b) again emphasizes the 2D character of the FS. The [001], [110], and [100] MCPs, shown in Figs. 3 and 4, involve a further integration

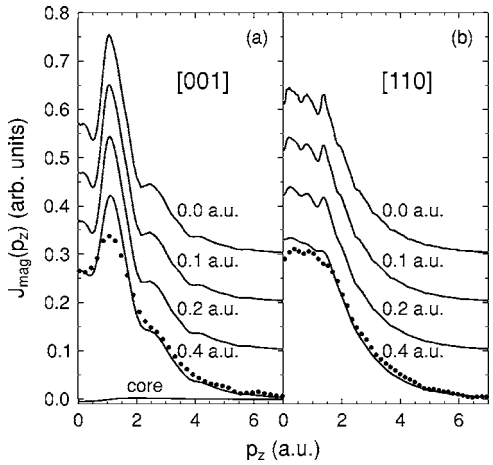

FIG. 3. Computed magnetic Compton profiles for the [001] and [110] directions in $La_{1.2}Sr_{1.8}Mn_2O_7$ convoluted with different resolution functions of indicated FWHM. The profiles include a small, isotropic core contribution shown separately at the bottom of (a). The dots give the experimental profiles at 7 T. The size of the dots is representative of the error bars on the data points. All profiles are normalized to the same area and have been offset vertically for clarity.

of the 2D projections of Fig. 2 along a high-symmetry direction. For example, the [100] MCP in Fig. 4 is obtained by projecting the 2D distribution of Fig. 2(a) onto the [100] (horizontal) axis, i.e., by integrating this density along the [010] direction. The MCPs in Figs. 3 and 4 include a small, isotropic contribution due to the polarization of the occupied core orbitals, which is given separately at the bottom of Fig. 3(a). We see at once that the high-density region in Fig. 2(a)

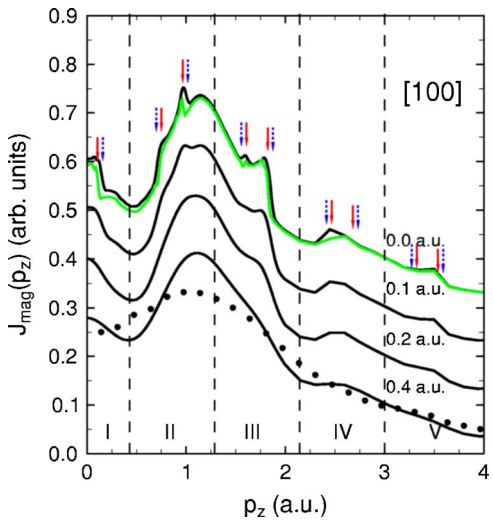

FIG. 4. (Color online) Central part of the computed magnetic Compton profiles for the [100] direction in $LaSr_2Mn_2O_7$ (green line) and $La_{1.2}Sr_{1.8}Mn_2O_7$ (black lines) convoluted with different resolution functions of indicated FWHM. The red (solid) and blue (dashed) arrows indicate the projected positions of the flat red and blue pieces of the doped Fermi surface in Fig. 1(b). Vertical dashed lines denote boundaries between the Brillouin zones numbered by the Roman numerals at the bottom.

centered around (1, 1 a.u.) projects into the peak extending over 0.5–1.8 a.u. in the [100] MCP in Fig. 4. This is also the case with the [001] MCP in Fig. 3(a), where one integrates the density of Fig. 2(b) over the horizontal direction. In sharp contrast, the [110] MCP requires an integration along a $[1\bar{1}0]$ direction in Fig. 2(a), which causes a broad peak centered around $p=0$ and spread over 0–1.8 a.u. in the [110] MCP in Fig. 3(b).[6,54]

In discussing baseline FS signatures in the MCPs it is best to focus on the unbroadened theory curves, which are the topmost curves in Figs. 3 and 4; we return to comment on the important role of resolution below. We first observe that due to the different projections of the magnetic momentum density involved in various profiles, the [100] profile is the only one expected to show significant FS structure. We therefore turn to Fig. 4, which shows the [100] MCP on an expanded scale. As in Fig. 3, the black solid curves in Fig. 4 refer to $La_{1.2}Sr_{1.8}Mn_2O_7$. The green curve represents the unbroadened MCP for the undoped ($x=0.5$) compound. The figure shows that the effect of doping, corresponding to the addition of 0.2 electron/f.u., is to raise the MCP by a small amount to account for the extra added electrons. Beyond this, there are shifts in the FS related features, which are in accord with the changes in the FS dimensions discussed in connection with Fig. 1 above. The blue and red arrows give the positions at which the blue and red flat pieces of the Fermi surface (the large hole cylinders) in Fig. 1(b) project onto the [100] direction. The projected sides of the majority-spin electron pillar nearly coincide with those of the smaller of the two hole cylinders and are not shown separately. The vertical dashed lines show the BZ boundaries. The arrows in zone I indicate the FS breaks in the first BZ; all other arrows correspond to Umklapp processes in higher BZs. The hole cylinders should thus manifest themselves as depressed parts of the profile between the two neighboring pairs of arrows surrounding various BZ boundaries. This is seen indeed to be the case between the arrows around the boundary of zones I and II over 0.2–0.7 a.u. as well as between zones III and IV over 1.85–2.40 a.u. This depression is, however, less clear between zones II and III or between zones IV and V due to compensating effects of other peaks in the momentum density such as the peak from the filled t_{2g} states. These results further highlight the importance of the matrix element in shaping FS features. For example, the size of the break at 1.85 a.u. is much larger than at 1 or at 2.5 a.u.

We now turn to the question of resolution broadening. Figures 3 and 4 show how the computed MCPs and the FS signatures therein are affected by resolution broadening varying from 0–0.4 a.u. (FWHM) and how these theoretical predictions compare with the corresponding experimental results. Recalling that the resolution broadening in the present measurements is 0.4 a.u., we see that the computed and measured MCPs are in reasonably good overall accord along all three high-symmetry directions. The computations correctly reproduce the presence of the strong peak around 1.1 a.u. in the [100] and [001] MCPs in Figs. 4 and 3(a) as well as the rather flat behavior of the [110] MCP at low momenta in Fig. 3(b). Some of the theoretically predicted secondary structure is also recognizable in the measurements [e.g., the bump around 2.5 a.u. in Fig. 3(a)], but under the resolution of 0.4 a.u. most FS features in the MCPs are washed out as are other smaller structures [e.g., the three small peaks in Fig. 3(b) at low momenta].

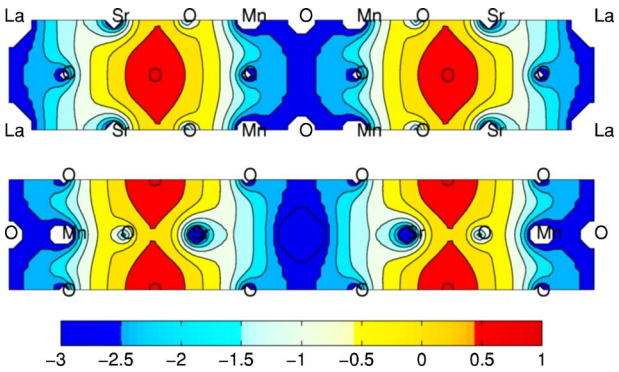

FIG. 5. (Color online) Logarithmic plot of the positron density in the planes $y=0$ (top) and $y=b/2$ (bottom) of the unit cell of $LaSr_2Mn_2O_7$. The c axis of the cell is drawn horizontally.

There are discrepancies as well between theory and experiment in Figs. 3 and 4. Notably, the computed peak in the [100] and [001] MCPs around 1.1 a.u. is stronger than the measured one. This difference reflects the limitations of the present LDA framework in treating correlation effects on the magnetic electrons in the system.[55–57] Electron correlations are known to broaden structure in Compton profiles and move momentum density from low to higher momenta.[5] They may also reduce the sizes of Fermi breaks in the momentum density in comparison to LSDA predictions. It is therefore important to establish whether the experimental results are resolution limited or not. A look at the different resolution broadened curves in Figs. 3 and 4 indicates that in order to obtain insight into this issue and to pin down FS features in the MCPs a resolution of 0.1 a.u. or better will be necessary.

D. Positron annihilation

In view of the similarity between the 2D projection of $\rho_{\mathrm{mag}}(\mathbf{p})$ in Fig. 2 and a polarized positron (e^+) 2D-ACAR distribution the interesting question arises whether the minority-spin pockets might be visible in a polarized positron measurement.[58] The 2D-ACAR technique avoids the second integration involved in Eq. (4) and possesses a superior momentum resolution (0.03–0.08 a.u.), enough to detect the minority-spin pillars, which have a diameter of 0.18 a.u. On the other hand, the positron does not sample the unit cell uniformly, and therefore, the positron wave function would need to overlap the Mn d_{xy} orbitals responsible for these pillars, in order to observe these pillars via the positron technique. A computation of the e^+ density shown in Fig. 5 finds that the positron does not entirely avoid the Mn d_{xy} orbitals, even though the greatest positron density is found between the SrO layers. A computation of the magnetic (001) 2D-ACAR distribution (not shown here), however, shows that the positron overlap with these Mn orbitals is indeed too low and that the minority-spin electron pillars are therefore not

observable in a polarized e^+ 2D-ACAR experiment. The majority-spin electron cylinders and pillars on the other hand are observable. A polarized e^+ 2D-ACAR experiment would be interesting in this connection.

V. SUMMARY AND CONCLUSIONS

We present all-electron first-principles computations of the magnetic momentum density $\rho_{\mathrm{mag}}(\mathbf{p})$ and MCPs along three high-symmetry directions in $LaSr_2Mn_2O_7$ and $La_{1.2}Sr_{1.8}Mn_2O_7$ within the LSDA-based band theory framework. Parallel measurements of these three MCPs from a single crystal of $La_{1.2}Sr_{1.8}Mn_2O_7$ at 5 K under a magnetic field of 7 T are also reported. The band structure is found to be that of a nearly half-metallic ferromagnet with a small minority-spin FS. The spin-polarized densities $\rho_\uparrow$ and $\rho_\downarrow$ are relatively smooth and structureless and are dominated by the large number of occupied bands. Their difference, $\rho_{\mathrm{mag}}(\mathbf{p})$, however, contains clear features due to the filled majority-spin t_{2g} states, the minority-spin counterparts of which lie above E_F. Insofar as FS signatures are concerned, imprints on the theoretical MCPs of the large squarish majority-spin hole sheets as well as those of the small minority-spin electron pillars are clearly seen spread throughout momentum space, although the intensity is generally small in the low momentum region due to the non-*s* character of the associated wave functions.

The quantity measured in a magnetic Compton scattering experiment is not $\rho_{\mathrm{mag}}(\mathbf{p})$, but the MCP $J_{\mathrm{mag}}(p_z)$, which is given by a double integral over p_x and p_y via Eq. (4). It is therefore important to understand how various magnetic orbitals and FS sheets will be reflected in the MCPs. We discuss this point in some detail. It turns out that the filled t_{2g} states of *xy*, *yz*, and *zx* symmetry continue to dominate the overall shape of the MCPs. These are responsible for the pronounced peaks around 1.1 a.u. in the [100] and the [001] MCP and also for the rather flat behavior of the [110] MCP over the 0–1.8 a.u. momentum range. Out of the five FS sheets in our band structure, only the large majority-spin hole cylinders yield a substantial fine structure in the computed [100] MCP; the [001] and [110] directions of the scattering vector are not favorable for investigating FS signatures in the MCP. The majority as well as the minority-spin electron pillars are barely visible in the MCPs and their observation through the magnetic Compton scattering technique will require reconstruction of the 2D or 3D magnetic momentum density from high resolution MCPs taken along a series of directions. The polarized positron annihilation 2D-ACAR experiment is also sensitive in observing some of these FS features.

The overall shapes and widths of the experimental MCPs along all three directions investigated are in good accord with theoretical predictions. In particular, the measured [100] and [001] MCPs display a pronounced peak around 1.1 a.u., while the [110] MCP is quite flat at low momenta, as is the case in the computed MCPs. A notable discrepancy is that the height of the measured peak around 1.1 a.u. in the [100] and [001] MCPs is smaller than the computed one, suggesting that electron correlation effects beyond the LSDA are needed to fully describe the magnetic electrons.[59] Some of the theoretically predicted fine structure is recognizable in the measured MCPs, but under the experimental resolution of 0.4 a.u., much of this structure including FS features is essentially washed out. Our analysis provides the momentum regions that deserve close scrutiny in order to detect Fermi surface related structure. It shows that a momentum resolution of about 0.1 a.u. or better is needed to pin down these FS features and other fine structure in the MCPs. It is clear that further magnetic Compton scattering measurements as well as polarized e^+ 2D-ACAR measurements on La manganites would be of great interest.

ACKNOWLEDGMENTS

We thank Hsin Lin for technical assistance in connection with this study. This work was supported by the US Department of Energy under Contracts No. DE-AC03-76SF00098 and DE-FG02-07ER46352. It was also sponsored by the Stichting Nationale Computer Faciliteiten for the use of supercomputer facilities, with financial support from the Netherlands Organization for Scientific Research (NWO), and benefited from the allocation of supercomputer time at the NERSC and the Northeastern University's Advanced Scientific Computation Center (NU-ASCC).

[1] Y. Moritomo, A. Asamitsu, H. Kuwahara, and Y. Tokura, Nature (London) **380**, 141 (1996).
[2] K. Hirota, Y. Moritomo, H. Fujioka, M. Kubota, H. Yoshizawa, and Y. Endoh, J. Phys. Soc. Jpn. **67**, 3380 (1998).
[3] P. M. Platzman and N. Tzoar, Phys. Rev. **139**, A410 (1965).
[4] N. Sakai and K. Ôno, Phys. Rev. Lett. **37**, 351 (1976).
[5] See, e.g., Y. Sakurai, Y. Tanaka, A. Bansil, S. Kaprzyk, A. T. Stewart, Y. Nagashima, T. Hyodo, S. Nanao, H. Kawata, and N. Shiotani, Phys. Rev. Lett. **74**, 2252 (1995); M. Itou, Y. Sakurai, T. Ohata, A. Bansil, S. Kaprzyk, Y. Tanaka, H. Kawata, and N. Shiotani, J. Phys. Chem. Solids **59**, 99 (1998).
[6] Y. Li, P. A. Montano, J. F. Mitchell, B. Barbiellini, P. E. Mijnarends, S. Kaprzyk, and A. Bansil, Phys. Rev. Lett. **93**, 207206 (2004).
[7] A. Koizumi, S. Miyaki, Y. Kakutani, H. Koizumi, N. Hiraoka, K. Makoshi, N. Sakai, K. Hirota, and Y. Murakami, Phys. Rev. Lett. **86**, 5589 (2001).
[8] A. Koizumi, T. Nagao, N. Sakai, K. Hirota, and Y. Murakami, Phys. Rev. B **74**, 012408 (2006).
[9] Assuming an independent-particle model in which the occupation function is one for an occupied state and zero for an unoccupied state.
[10] See, e.g., E. Żukowsky, in *X-Ray Compton Scattering*, edited by M. J. Cooper, P. E. Mijnarends, N. Shiotani, N. Sakai, and A. Bansil (Oxford University Press, Oxford, 2004), p. 148.
[11] N. Sakai, O. Terashima, and H. Sekizawa, Nucl. Instrum. Meth-

ods Phys. Res. A **221**, 419 (1984).
[12] P. A. Montano, G. S. Knapp, G. Jennings, E. Gluskin, E. Trakhtenberg, I. B. Vasserman, P. M. Ivanov, D. Frachon, E. R. Moog, L. R. Turner, G. K. Shenoy, M. J. Bedzyk, M. Ramanathan, M. A. Beno, and P. L. Cowan, Rev. Sci. Instrum. **66**, 1839 (1995).
[13] P. K. de Boer and R. A. de Groot, Phys. Rev. B **60**, 10 758 (1999).
[14] Reference 13 also reports computations on $LaSr_2Mn_2O_7$ in the form of a slab terminated in an SrO layer.
[15] R. Seshadri, A. Maignan, M. Hervieu, N. Nguyen, and B. Raveau, Solid State Commun. **101**, 453 (1997).
[16] J. P. Perdew, J. A. Chevary, S. H. Vosko, K. A. Jackson, M. R. Pederson, D. J. Singh, and C. Fiolhais, Phys. Rev. B **46**, 6671 (1992).
[17] X. Y. Huang, O. N. Mryasov, D. L. Novikov, and A. J. Freeman, Phys. Rev. B **62**, 13 318 (2000).
[18] Note that our definition of x is different from that of Ref. 17.
[19] M. Kubota, H. Fujioka, K. Hirota, K. Ohoyama, Y. Moritomo, H. Yoshizawa, and Y. Endoh, J. Phys. Soc. Jpn. **69**, 1606 (2000).
[20] M. Methfessel, Phys. Rev. B **38**, 1537 (1988).
[21] M. Methfessel, C. O. Rodriguez, and O. K. Andersen, Phys. Rev. B **40**, R2009 (1989).
[22] D. M. Ceperley and B. J. Alder, Phys. Rev. Lett. **45**, 566 (1980).
[23] D. S. Dessau (private communication).
[24] W. E. Pickett and D. J. Singh, Phys. Rev. B **53**, 1146 (1996).
[25] D. J. Singh and W. E. Pickett, Phys. Rev. B **57**, 88 (1998).
[26] E. O. Wollan and W. C. Koehler, Phys. Rev. **100**, 545 (1955).
[27] E. A. Livesay, R. N. West, S. B. Dugdale, G. Santi, and T. Jarlborg, J. Phys.: Condens. Matter **11**, L279 (1999).
[28] B. Nadgorny, I. I. Mazin, M. Osofsky, R. J. Soulen, Jr., P. Broussard, R. M. Stroud, D. J. Singh, V. G. Harris, A. Arsenov, and Ya. Mukovskii, Phys. Rev. B **63**, 184433 (2001).
[29] S. Kaprzyk and A. Bansil, Phys. Rev. B **42**, 7358 (1990).
[30] A. Bansil and S. Kaprzyk, Phys. Rev. B **43**, 10335 (1991).
[31] A. Bansil, S. Kaprzyk, and J. Toboła, in *Applications of Multiple Scattering Theory in Material Science*, edited by W. H. Butler, P. H. Dederichs, A. Gonis, and R. L. Weaver, Mat. Res. Soc. Symp. Proc. 253, p. 505 (Materials Research Society, Pittsburgh, 1992).
[32] A. Bansil, S. Kaprzyk, P. E. Mijnarends, and J. Toboła, Phys. Rev. B **60**, 13396 (1999).
[33] In our computations the core states are treated relativistically, but the valence electrons are treated semirelativistically.
[34] P. E. Mijnarends and A. Bansil, Phys. Rev. B **13**, 2381 (1976).
[35] P. E. Mijnarends and A. Bansil, Phys. Rev. B **19**, 2912 (1979).
[36] P. E. Mijnarends and A. Bansil, J. Phys.: Condens. Matter **2**, 911 (1990).
[37] A. Bansil, R. S. Rao, P. E. Mijnarends, and L. Schwartz, Phys. Rev. B **23**, 3608 (1981).
[38] P. E. Mijnarends and A. Bansil, in *Positron Spectroscopy of Solids*, edited by A. Dupasquier and A. P. Mills (IOS Press, Amsterdam, 1995), p. 25.
[39] X-ray and neutron scattering experiments have revealed superlattice reflections associated with the formation of polarons in the paramagnetic phase. However, such polaronic effects appear to collapse at low T and in the presence of high magnetic fields [see L. Vasiliu-Doloc, S. Rosenkranz, R. Osborn, S. K. Sinha, J. W. Lynn, J. Mesot, O. H. Seeck, G. Preosti, A. J. Fedro, and J. F. Mitchell, Phys. Rev. Lett. **83**, 4393 (1999)]. Notably, the superlattice peaks collapse in intensity at T_c [see D. N. Argyriou, J. W. Lynn, R. Osborn, B. Campbell, J. F. Mitchell, U. Ruett, H. N. Bordallo, A. Wildes, and C. D. Ling, *ibid.* **89**, 036401 (2002)].
[40] The use of $l_{max}=2$ for Mn would truncate the central majority-spin pillar to an ellipsoid.
[41] U. von Barth and L. Hedin, J. Phys. C **5**, 1629 (1972); A. K. Rajagopal and J. Callaway, Phys. Rev. B **7**, 1912 (1973).
[42] The full-potential computations performed by us also yield a slightly occupied minority-spin conduction band.
[43] In order to accurately reproduce the dispersion of the FS sheets, the calculation of the Fermi surface was based on a dense mesh of 2805 **k** points in the irreducible wedge of the BZ.
[44] B. J. Campbell, R. Osborn, D. N. Argyriou, L. Vasiliu-Doloc, J. F. Mitchell, S. K. Sinha, U. Ruett, C. D. Ling, Z. Islam, and J. W. Lynn, Phys. Rev. B **65**, 014427 (2001).
[45] Y.-D. Chuang, A. D. Gromko, D. S. Dessau, T. Kimaura, and Y. Takura, Science **292**, 1509 (2001).
[46] I. Matsumoto, J. Kwiatkowska, F. Maniawski, M. Itou, H. Kawata, N. Shiotani, S. Kaprzyk, P. E. Mijnarends, B. Barbiellini, and A. Bansil, Phys. Rev. B **64**, 045121 (2001).
[47] See, e.g., R. N. West, in *Positron Spectroscopy of Solids*, edited by A. Dupasquier and A. P. Mills (IOS Press, Amsterdam, 1995), p. 75.
[48] J. R. Schneider, F. Bell, Th. Tschentscher, and A. J. Rollason, Rev. Sci. Instrum. **63**, 1119 (1992).
[49] F. Bell, Th. Tschentscher, J. R. Schneider, and A. J. Rollason, J. Phys.: Condens. Matter **3**, 5587 (1991).
[50] Th. Tschentscher, J. R. Schneider, F. Bell, A. J. Rollason, and M. B. J. Woolf, Nucl. Instrum. Methods Phys. Res. B **79**, 237 (1993).
[51] The momentum density of a d state behaves as p^4 at small p.
[52] R. Harthoorn and P. E. Mijnarends, J. Phys. F: Met. Phys. **8**, 1147 (1978).
[53] Since the projected magnetic momentum density in the little circles is smaller than the surrounding density, the contribution of the minority-spin pillars clearly outweighs that of the majority-spin pillars.
[54] The increased difference at low momenta between theory and experiment with respect to Fig. 2 of Ref. 6 is the result of doping.
[55] It should be noted that the present computation does not include a Lam-Platzman (Ref. 56) correction to take into account electron-electron correlation. It is not clear how the Lam-Platzman type correction can be generalized to treat the magnetic momentum density.
[56] L. Lam and P. M. Platzman, Phys. Rev. B **9**, 5122 (1974).
[57] I. G. Kaplan, B. Barbiellini, and A. Bansil, Phys. Rev. B **68**, 235104 (2003).
[58] K. E. H. M. Hanssen, P. E. Mijnarends, L. P. L. M. Rabou, and K. H. J. Buschow, Phys. Rev. B **42**, 1533 (1990).
[59] Of course, other effects such as possible deformations associated with polaronic effects may be involved in these discrepancies [see S. Miyaki, S. Uzuhara, K. Terada, K. Makoshi, and H. Koizumi, Phys. Rev. B **71**, 085117 (2005)].